

1 International Journal of Modern Physics A  
 2 © World Scientific Publishing Company

3 **STUDY OF THE CENTRAL EXCLUSIVE PRODUCTION OF  $\pi^+\pi^-$ ,**  
 4  **$K^+K^-$ , AND  $p\bar{p}$  PAIRS IN PROTON-PROTON COLLISIONS AT**  
 5  **$\sqrt{s} = 510$  GEV WITH THE STAR DETECTOR AT RHIC.**

6 TOMÁŠ TRUHLÁŘ\*

7 *Faculty of Nuclear Sciences and Physical Engineering, Czech Technical University in Prague,*  
 8 *Address*

9 *Brehova 78/7, Prague 115 19, Czech Republic*  
 10 *Tomas.Truhlar@fjfi.cvut.cz*

11 Received Day Month Year

12 Revised Day Month Year

13 We report on the measurement of the central exclusive production process  $pp \rightarrow pXp$   
 14 in proton-proton collisions at  $\sqrt{s} = 510$  GeV with the STAR detector at RHIC. At this  
 15 energy, the process is dominated by a double Pomeron exchange mechanism. The tracks of  
 16 the centrally produced system  $X$  were reconstructed in the central detector of STAR, the  
 17 time projection chamber and the time of flight systems. Particles were identified using the  
 18 ionization energy loss and the time of flight method. The diffractively scattered protons,  
 19 moving intact inside the RHIC beam pipe after the collision, were measured in the Roman  
 20 Pots system allowing full control of the interaction's kinematics and verification of its  
 21 exclusivity. Preliminary results on the invariant mass distributions of centrally produced  
 22  $\pi^+\pi^-$ ,  $K^+K^-$ , and  $p\bar{p}$  pairs measured within the STAR acceptance are presented.

23 *Keywords:* Double Pomeron exchange; STAR; Roman Pots.

24 PACS numbers:

25 **1. Introduction**

26 Central Exclusive Production<sup>1</sup> (CEP) through double Pomeron exchange is consid-  
 27 ered to be a gluon rich process. Thus, it is suitable to look for hadronic production of  
 28 glueballs,<sup>2</sup> bound states consisting only of gluons, predicted by non-Abelian nature  
 29 of quantum chromodynamics. The CEP of two hadrons is a process, where protons  
 30 stay intact and a central state is produced with quantum numbers of vacuum and is  
 31 well separated from outgoing protons by rapidity gaps. A generic diagram of CEP  
 32 with resonance and continuum production is shown in Fig. 1. The CEP mechanism,  
 33 where two Pomerons are exchanged, is considered to be dominant at the Relativistic  
 34 Heavy Ion Collider<sup>3</sup> (RHIC) energy.<sup>4</sup> Although, this process is the simplest four  
 35 body quantum chromodynamics process, it is theoretically very complex due to

\*For the STAR Collaboration.

2 *T. Truhlář*

36 significant interference effects between resonance and continuum production. Fur-  
 37 thermore, there may be significant rescattering effects via additional interactions  
 38 between the protons.

39 GRANIITTI<sup>5</sup> is a Monte Carlo event generator for high energy diffraction cap-  
 40 able to describe both resonance and continuum production in CEP. Presented  
 41 results are compared to the newest tune of GRANIITTI, version 1.080, with added  
 42 CEP resonance couplings also tuned to STAR results from proton-proton colli-  
 43 sions at  $\sqrt{s} = 200$  GeV,<sup>4</sup> the highest center-of-mass energies at which the double  
 44 Pomeron exchange has been measured with the detection of the forward-scattered  
 45 protons. The following resonances were included in the resonance production:  
 46  $f_0(500)$ ,  $\rho(770)$ ,  $f_0(980)$ ,  $\phi(1020)$ ,  $f_2(1270)$ ,  $f_0(1500)$ ,  $f_2(1525)$ , and  $f_0(1710)$ .  
 47 Significant interference effects between resonance and continuum production are  
 48 taken into account.

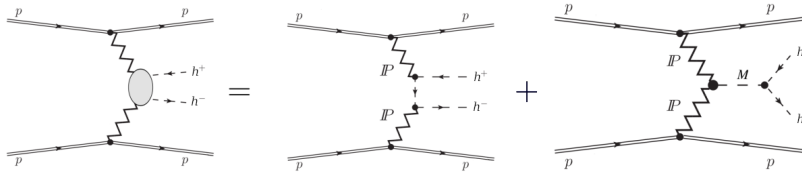


Fig. 1. A generic diagram of central exclusive production of two hadron as combination of con-  
 tinuum and resonance production.

## 49 2. Experimental setup

50 The Solenoidal Tracker at RHIC<sup>6</sup> (STAR) is a multi-purpose detector consisting of  
 51 many sub-detectors, allowing measurement and identification of charged particles.  
 52 In the Time Projection Chamber<sup>7</sup> (TPC), charged particles are tracked and their  
 53 energy loss as a function of their momenta is measured in pseudorapidity  $|\eta| < 1$  and  
 54 full azimuthal angle. In combination with measuring the time-of-flight information  
 55 in the Time Of Flight<sup>8</sup> (TOF) system, STAR enables precise particle identification.  
 56 Forward rapidity Beam-Beam Counters<sup>9</sup> (BBC), covering  $2.1 < |\eta| < 5.0$ , are used  
 57 to ensure rapidity gaps. A schematic view of the STAR detector with highlighted  
 58 main sub-detectors can be seen in Fig. 2. In addition, the STAR experiment has  
 59 forward silicon strip detectors installed in Roman Pots<sup>10</sup> at 15.8 and 17.6 meters  
 60 on both sides of the interaction point. In each Roman Pot, a package of four silicon  
 61 strip detectors and a scintillation trigger counter is installed giving spatial resolution  
 62 of  $30 \mu\text{m}$  and active area of  $79 \times 49 \text{ mm}^2$ . Figure 3 shows the layout of all eight  
 63 Roman Pot detectors allowing to measure forward-scattered protons' momenta and  
 64 therefore verification of interaction's exclusivity.

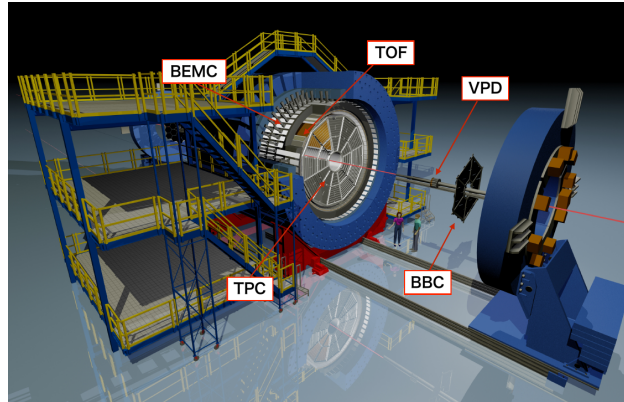


Fig. 2. A schematic view of the STAR detector, main sub-detectors are highlighted.

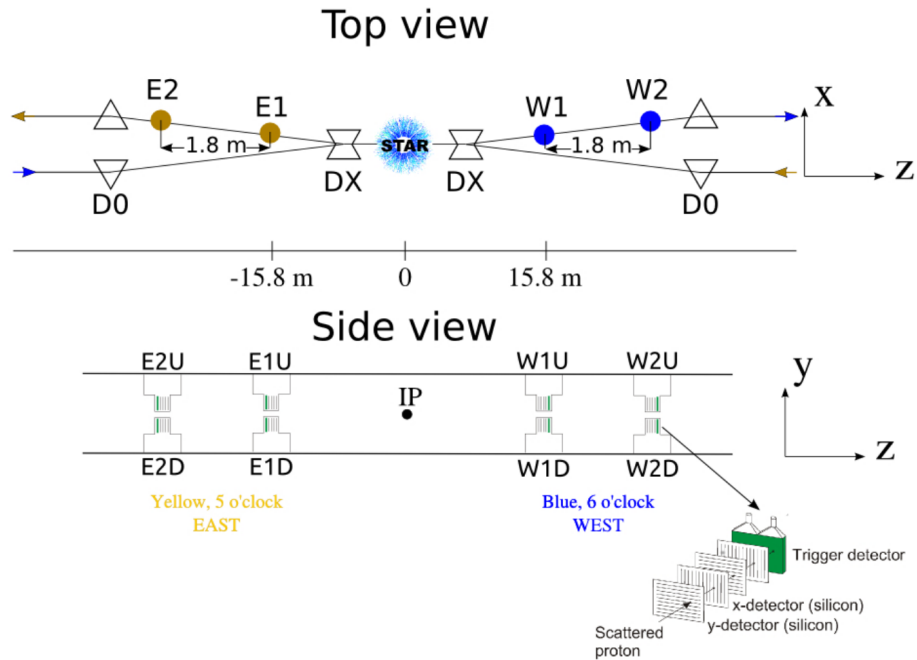


Fig. 3. The Roman Pot system. Top view shows Roman Pot stations E1, E2, W1, W2 and dipole magnets DX, D0 installed on both sides of the central detector. Side view illustrates individual Roman Pots consisting from four Silicon Strip Detector package and a scintillation counter.

### 65 3. Data sample and event selection

66 In 2017, the STAR experiment measured proton-proton collisions at  $\sqrt{s} = 510$  GeV.  
 67 More than 620 million events from these collisions were collected and analysed. The  
 68 events were triggered on a signal in the Roman Pot detectors on both side of the

4 *T. Truhlář*

69 STAR detector. Moreover, the trigger required low TOF multiplicity and a veto  
 70 on BBC signal to ensure the double rapidity gap topology characteristic for CEP  
 71 events. A sample of CEP candidate events was obtained by applying the selection  
 72 criteria listed below.

73 First, only events with one forward-scattered proton on each side are selected. In  
 74 addition, all eight silicon strip detectors have to be used in the proton reconstruction  
 75 to ensure good quality of the proton track. Furthermore, the proton transverse  
 76 momentum is required to be inside a fiducial region to ensure pure geometrical  
 77 acceptance. The fiducial region is illustrated by black lines in Fig. 4 (left) and listed  
 78 in legends of Figs. 6, 7, and 8.

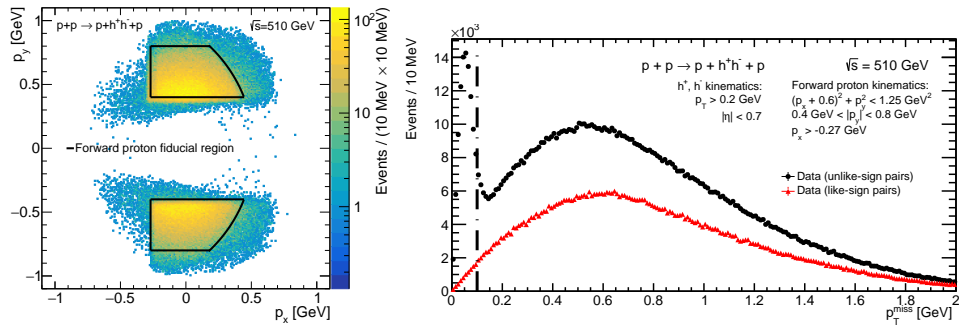


Fig. 4. Left: The distribution of reconstructed proton momenta. The black contours indicate the fiducial region used in the analysis. Right: The distribution of the missing transverse momentum  $p_T^{miss}$  for CEP event candidates with the used cut ( $p_T^{miss} < 100$  MeV) illustrated by the black dot-dashed line.

79 Second, only events with exactly two primary TPC tracks matched with two  
 80 TOF hits and originating from the same vertex are selected. Next, track quality  
 81 cuts are applied on the number of hits used in the track reconstruction and on  
 82 the number of hits used for measuring the energy loss. To ensure high geometrical  
 83 acceptance for the central tracks in the entire fiducial phase space, further criteria  
 84 are used: a cut on the  $z$ -position of the vertex ( $|z\text{-position of vertex}| < 80$  cm) and  
 85 a cut on pseudorapidity of central tracks ( $|\eta| < 0.7$ ).

86 Third, a cut on missing transverse momenta  $p_T^{miss}$  ( $p_T^{miss} < 100$  MeV) is applied  
 87 to ensure exclusivity of the event. The  $p_T^{miss}$  is the transverse momentum of the  
 88 sum of of all measured particles and it should be equal to zero for the CEP due  
 89 to conservation of momentum. Figure 4 (right) depicts the distribution of  $p_T^{miss}$  for  
 90 CEP event candidates with the used cut.

91 Finally, particle identification is done based on combined information from the  
 92 TPC, the energy loss, and TOF ( $m_{\text{TOF}}^2$ ). The  $m_{\text{TOF}}^2$ , as determined from TOF, is the  
 93 squared invariant mass of a particle type ( $\pi$ ,  $K$ , and  $p$ ). Details on the computation  
 94 of  $m_{\text{TOF}}^2$  can be found in Appendix A. In addition, more restrictive cuts on track  
 95 momenta are imposed to provide high purity of the pair sample. These cuts are

96 listed in legends of Figs. 6, 7, and 8. Figure 5 shows the energy loss of charged  
 97 particles as a function of their momenta (left) and the distribution of  $m_{TOF}^2$  for  
 98 exclusive events (right), where peaks of pions, kaons, and protons about their real  
 99 mass squared values can be seen.

100 In the end, 62077  $\pi^+\pi^-$ , 1697  $K^+K^-$ , and 125  $p\bar{p}$  CEP event candidates were  
 101 obtained after applying all the selection criteria mentioned above.

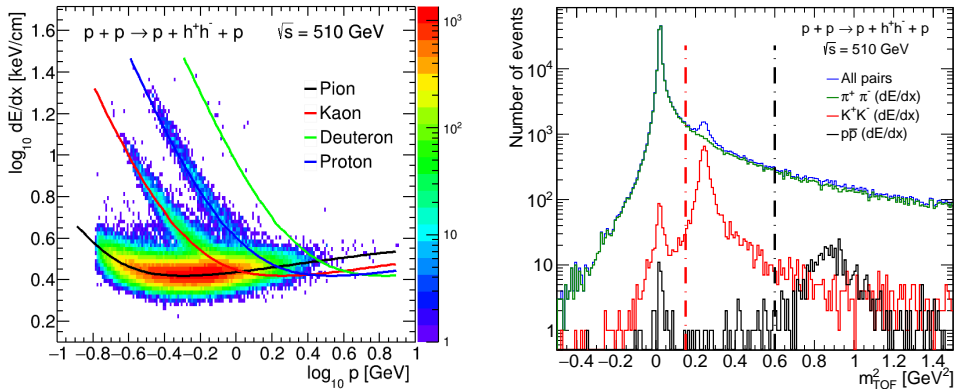


Fig. 5. Left: The energy loss of charged particles as a function of their momenta for exclusive events. Theoretical predictions for pions, kaons, protons, and deuterons are depicted by coloured curves. Right: The distribution of  $m_{TOF}^2$  for exclusive pairs and for  $\pi^+\pi^-$ ,  $K^+K^-$ , and  $p\bar{p}$  pairs determined solely from the energy loss. Dot-dash lines indicate used  $m_{TOF}^2$  cuts.

#### 102 4. Results

103 In Figs. 6 and 7, invariant mass distributions of selected centrally produced  $\pi^+\pi^-$ ,  
 104  $K^+K^-$ , and  $p\bar{p}$  pairs measured within the STAR acceptance in proton-proton col-  
 105 lisions at  $\sqrt{s} = 510$  GeV are shown. All presented invariant mass distributions were  
 106 corrected for the detector acceptance using the pure single particle STAR detector  
 107 simulation. Also, they were normalized such that the area under the distribution  
 108 is equal to one. The error bars represent statistical uncertainties only and natural  
 109 units were used.

110 The invariant mass distribution of  $\pi^+\pi^-$  pairs shows expected features: a drop  
 111 at about 1 GeV, possibly due to the negative interference of  $f_0(980)$  with the con-  
 112 tinuum contribution, and a peak consistent with the  $f_2(1270)$ . In the invariant mass  
 113 of  $K^+K^-$ , a peak at about 1.5 GeV, possible  $f_2(1525)$ , and a strong enhancement  
 114 at about 1.5 GeV, possible  $f_0(980)$  or  $\phi(1020)$ , are seen. The invariant mass of  $p\bar{p}$   
 115 does not show any resonances. In general, GRANIITTI can describe shapes of dis-  
 116 tributions. Even the strong enhancement at a mass about 1 GeV for  $K^+K^-$  pairs is  
 117 predicted by GRANIITTI, while the enhancement is not seen and it is not predicted  
 118 in fiducial region of STAR measurement at  $\sqrt{s} = 200$  GeV.<sup>4</sup>

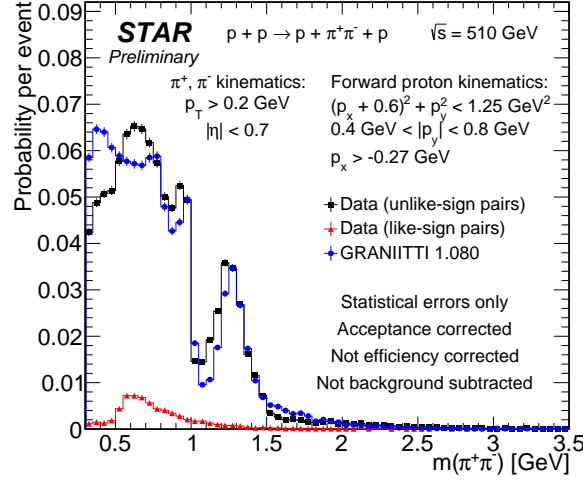
6 *T. Truhlář*


Fig. 6. The acceptance corrected invariant mass spectrum of exclusively produced  $\pi^+\pi^-$  pairs. Results are compared with the newest tune of GRANIITTI,<sup>5</sup> version 1.080. Error bars represent the statistical uncertainties.

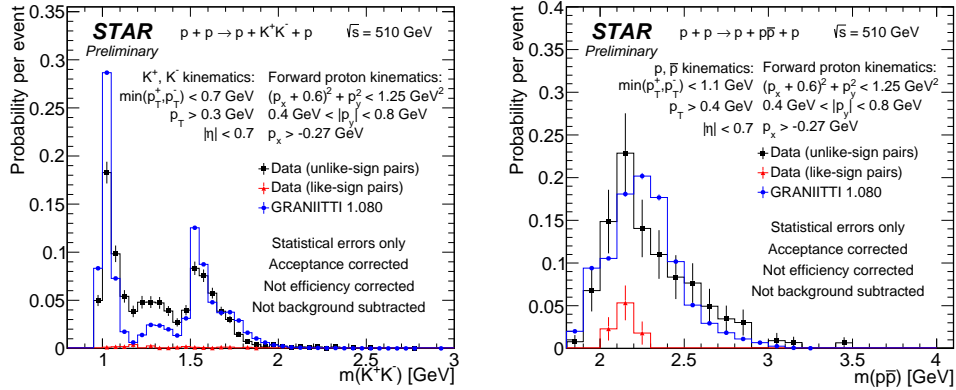


Fig. 7. Acceptance corrected invariant mass spectra of exclusively produced  $K^+K^-$  pairs (left) and  $p\bar{p}$  pairs (right). Results are compared with a new tune of GRANIITTI,<sup>5</sup> version 1.080. Error bars represent the statistical uncertainties.

119 The invariant mass distribution of selected  $\pi^+\pi^-$  pairs is differentiated in two  
 120 regions of  $\Delta\varphi$ ,  $\Delta\varphi < 90^\circ$  and  $\Delta\varphi > 90^\circ$ , where  $\Delta\varphi$  is the difference between the  
 121 azimuthal angles of the forward protons. The selection of events with  $\Delta\varphi > 90^\circ$   
 122 could act as a glueball filter<sup>11</sup> since the production of quark-antiquark states is  
 123 suppressed compared to glueballs in the limit  $|\vec{p}_{1,T} - \vec{p}_{2,T}| \rightarrow 0$  corresponding to  
 124 the limit  $\Delta\varphi \rightarrow 180^\circ$ .

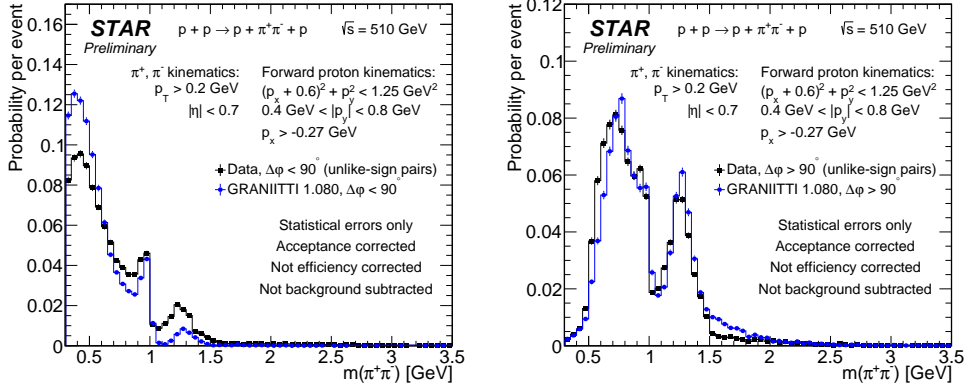


Fig. 8. The acceptance corrected invariant mass spectrum of exclusively produced  $\pi^+\pi^-$  pairs differentiated in two regions of the difference of azimuthal angles of the forward protons:  $\Delta\varphi < 90^\circ$  (left) and  $\Delta\varphi > 90^\circ$  (right). Results are compared with a new tune of GRANIITTI,<sup>5</sup> version 1.080. Error bars represent the statistical uncertainties.

## 125 5. Summary

126 The preliminary STAR results on CEP of charged particle pairs produced in proton-  
 127 proton collisions at  $\sqrt{s} = 510$  GeV with measured forward-scattered protons have  
 128 been presented.

129 The results confirm features seen in previous experiments even though new fea-  
 130 tures are seen, like the peak at the invariant mass of about 1 GeV for  $K^+K^-$  pairs.  
 131 The results were compared with the newest tune of the Monte Carlo event gener-  
 132 ator, GRANIITTI, that can describe the shape of the data quite well suggesting  
 133 significant role of resonance production.

## 134 Acknowledgments

135 This work was supported from the project LTT18002 of the Ministry of Education,  
 136 Youth, and Sport of the Czech Republic and from European Regional Development  
 137 Fund-Project "Center of Advanced Applied Science" No. CZ.02.1.01/0.0/0.0/16-  
 138 019/0000778.

## 139 Appendix A. The $m_{\text{TOF}}^2$ method

140 The  $m_{\text{TOF}}^2$  method is based on the assumption that two hadron of the same type  
 141 (same mass) are produced from the same vertex. Then, their masses squared can  
 142 be derived. Assuming that two hadrons are produced in the same vertex at time  $t_0$   
 143 and they are detected in the TOF detector at time  $t_1$  and  $t_2$ . Then, we can write  
 144 following equations:

$$t_1 - t_0 = L_1 \sqrt{1 + \frac{m_1^2}{p_1^2}}, \quad (\text{A.1})$$

8 *T. Truhlář*

145

$$t_2 - t_0 = L_2 \sqrt{1 + \frac{m_2^2}{p_2^2}}, \quad (\text{A.2})$$

146 where  $p_1$  and  $p_2$  are momenta and  $L_1$  and  $L_2$  are lengths of the first and the second  
147 central track. The time  $t_0$  can be removed by subtracting A.2 from ??:

$$\Delta t = t_1 - t_2 = L_1 \sqrt{1 + \frac{m_1^2}{p_1^2}} - L_2 \sqrt{1 + \frac{m_2^2}{p_2^2}}. \quad (\text{A.3})$$

148 Since we assume the two particles have the same mass, we can write  $m_1^2 = m_2^2 =$   
149  $m_{\text{TOF}}^2$  and transform A.3 into a quadratic equation in the following form:

$$A \cdot (m_{\text{TOF}}^2)^2 + B \cdot m_{\text{TOF}}^2 + C = 0, \quad (\text{A.4})$$

150 where parameters  $A$ ,  $B$ , and  $C$  are defined as follows:

$$A = -2 \frac{L_1^2 L_2^2}{p_1^2 p_2^2} + \frac{L_1^4}{p_1^4} + \frac{L_2^4}{p_2^4}, \quad (\text{A.5})$$

151

$$B = -2L_1^2 L_2^2 \left( \frac{1}{p_1^2} + \frac{1}{p_2^2} \right) + 2 \frac{L_1^4}{p_1^4} + 2 \frac{L_2^4}{p_2^4} - 2(\Delta t)^2 \left( \frac{L_1^2}{p_1^2} + \frac{L_2^2}{p_2^2} \right), \quad (\text{A.6})$$

152

$$C = (\Delta t)^4 - 2(\Delta t)^2(L_1^2 + L_2^2) + L_1^4 + L_2^4 - 2L_1^2 L_2^2. \quad (\text{A.7})$$

153 Finally,  $m_{\text{TOF}}^2$  can be determined using the formula:

$$m_{\text{TOF}}^2 = \frac{-B + \sqrt{B^2 - 4AC}}{2A}. \quad (\text{A.8})$$

## 154 References

- 155 1. M. G. Albrow, T.D. Coughlin and J.R. Forshaw, *Prog. Part. Nucl. Phys.* **65**, 149 (2010).
- 156 2. K. Ishikawa, G. Schierholz and M. Teper, *Z. Phys. C* **19**, 327 (1983).
- 157 3. H. Hahn *et al.*, *Nucl. Instrum. Meth.* **499**, 245 (2003).
- 158 4. STAR Collaboration, (J. Adam *et al.*), *JHEP* **07**, 178 (2020).
- 159 5. M. Mieskolainen, *arXiv:1910.06300*
- 160 6. STAR Collaboration, (K. H. Ackermann *et al.*), *Nucl. Instrum. Meth.* **499**, 624 (2003).
- 161 7. M. Anderson *et al.*, *Nucl. Instrum. Meth.* **499**, 659 (2003).
- 162 8. STAR Collaboration, (J. Wu *et al.*), *J. Phys. G* **34**, 729 (2007).
- 163 9. STAR Collaboration, (C. A. Whitten *et al.*), *AIP Conf. Proc.* **980**, 1 (2008).
- 164 10. S. Bultmann *et al.*, *Nucl. Instrum. Meth.* **535**, 415 (2004).
- 165 11. F. E. Close and A. Kirk, *Nucl. Instrum. Meth.* **397**, 3 (1997).